APPENDIX B

INTERFEROMETER CONCEPTS AND NOISE

This appendix provides some analytic basis and further explanations for the concepts introduced in Section III. The subjects discussed are

1. The theory of the Fabry-Perot Cavity
2. The transfer function of an interferometric gravitational wave detector
3. Basic optical concepts including the RF phase modulation of the optical beams
4. The physical basis of some of the noise terms

There is an extensive published literature on these issues [B–1]. We include a discussion of them here for the sake of completeness of the proposal.

1. The Theory of the Fabry-Perot Cavity.

In a gravitational wave interferometer each arm's Fabry-Perot cavity is a light storage element. The input mirror, in the interferometer corner station, is partially transmitting with an intensity transmission coefficient of $T_1 = (1 - R_1 - A_1)$. Here A_1 is the mirror's optical absorption and R_1 is its intensity reflection coefficient. The rear mirror, which is in one of the interferometer's end stations a distance L from the input mirror, is coated for high reflectivity, $R_2 = (1 - A_2) \approx 1$, i.e. for negligible transmission. The electric field reflection and transmission coefficients of each mirror, $r_1,\ r_2,\ t_1,\ t_2$ are equal to the square root of the intensity coefficients; the reflection coefficients have opposite sign depending on whether the incident beam approaches the reflecting surface from the substrate side or from the vacuum.

When an optical electric field pulse of unit amplitude is incident on the cavity input mirror, a set of pulses is returned from the cavity. Figure B–1a shows the time series of these pulses. The first pulse, reflected by the input mirror, returns immediately and has an amplitude of r_1. The second pulse, reflected once by the rear mirror where it is inverted in sign, arrives a time $2L/c$ later and is reduced in amplitude to $r_2 t_1 t_1$ as a result of two transmissions through the input mirror and one reflection off the end mirror. Subsequent pulses undergo reflections from both mirrors and are delayed in time by $n2L/c$ where n is the number of round trips in the cavity. The pulses become progressively smaller and have amplitudes $t_1 t_1 r_2 (r_1 r_2)^n$. The sum of all these pulses is the cavity's "reflected electric field impulse response" (Green's function), and is given algebraically by

$$h_R(t) = \frac{E_R(t)}{E_0} = r_1 \delta(t) - t_1 t_1 r_2 \sum_{n=0}^{\infty} (r_1 r_2)^n \delta\left(\frac{t - 2L(n+1)}{c}\right). \qquad \text{(B.1)}$$

The response of the cavity for an arbitrary incident electric field is the convolution

of the impulse response with the incident field.

$$E_R(t) = \int_{-\infty}^{t} h_R(\tau) E_{\rm inc}(t-\tau) d\tau.$$

If the input light has a sinusoidal dependence, $E_{inc}(t-\tau) = E_0 e^{i\omega(t-\tau)}$, the convolution gives the cavity's reflection transfer function:

$$\frac{E_r(t)}{E_o} = e^{i\omega t}\Big[r_1 - t_1 t_1 r_2 \;\; e^{-i2\omega L/c} \sum_{n=0}^{\infty} (r_1 r_2)^n \;\; e^{-i2\omega n L/c}\Big]. \tag{B.2}$$

Since $|r_1 r_2| < 1$ the series can be summed:

$$\begin{aligned} \frac{E_r(t)}{E_o} &= e^{i\omega t}\left[r_1 - \frac{t_1 t_1 r_2 \; e^{-i2\omega L/c}}{1 - r_1 r_2 \; e^{-i2\omega L/c}}\right] \\ &= e^{i\omega t}\left[\frac{r_1 - r_2(r_1^2 + t_1^2) \; e^{-i2\omega L/c}}{1 - r_1 r_2 \; e^{-i2\omega L/c}}\right]. \end{aligned} \tag{B.3}$$

Figure B–1b, a phasor diagram, shows how the convolution produces the reflection transfer function of the cavity. The resultant field is made up from the superposition of the individual waves from the multiple reflections described in Figure B–1, (a). The net reflected electric field is the distance from the origin, the center of the circle, to the end point of a trajectory indicated by a progression of dots. The phase of the net reflected field is the azimuthal angle around the circle with zero degrees being to the right. Each trajectory, associated with a specific value of $x = (2\omega L/c) - (2\omega_0 L_0/c)$, begins at the point marked by $*$ which represents the first term in the series: the initial reflection from the input mirror. Along any one trajectory the distance between dots is proportional to the magnitude of the individual reflected components. The angle of each line segment between dots, relative to the horizontal, is the phase of the individual reflected wave. The trajectory labeled $x = 0$ is the resonance case, with cavity length equal to a half integral multiple of the laser wavelength. Going to the left one sees the individual reflections adding up coherently with the resultant field being almost equal to the incident field but shifted in phase by 180 degrees providing the cavity losses are small. In a low loss cavity, the component of the field emerging from the cavity is almost twice the incident field. As the cavity is moved away from resonance, $x \neq 0$, by a change in length, the phase of the net reflected wave changes; this phase shift is proportional to an incident gravitational wave. The change in net phase produced by a unit change in cavity length is a maximum at resonance. At large values of x, far from resonance, the phase of the successive individual waves changes rapidly and the phase of the resultant reflected field changes little with a change in x. The entire cavity then behaves just like the input mirror without a cavity behind it.

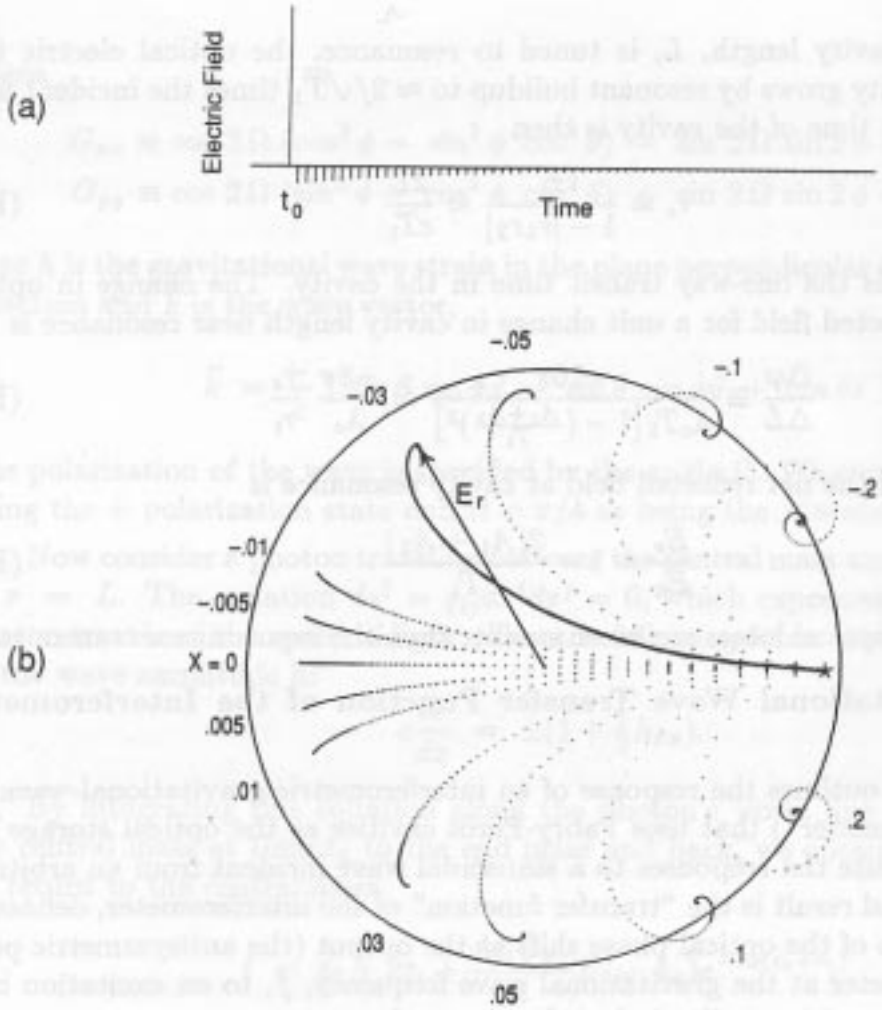

Figure B–1 (a) Time evolution of the optical response of a Fabry–Perot cavity to an input pulse. The figure is drawn for a cavity with an input mirror transmission $T = 0.1$, end mirror reflectivity $R = 1$, and 0.01 loss per pass in the cavity mirrors. The direct reflection from the input mirror occurs at time t_0. The delayed pulses (with opposite phase from the initial one) correspond to light which enters the cavity, and reflects many times between the mirrors; a small amount of this light is transmitted upon each encounter with the input mirror. (b) Phasor diagram for light reflected from a Fabry-Perot cavity with the same properties, under continuous illumination. The radius of the circle is equal to the amplitude of the input light beam. The direct reflection from the input mirror is the vector (not drawn) from the center of the circle to the star. Each series of dots, originating at the star, represents the superposition of waves which have made different numbers of passes through the cavity, calculated for a given value of detuning between the input light and the cavity's resonance frequency. The length and direction of each line segment connecting adjacent dots corresponds to the amplitude and phase, respectively, of one of these waves. The vector from the origin to the end of the series (E_r) gives the net electric field reflected from the cavity. The vector from the star to the end of the series (not drawn) is the leakage field from the cavity.

The light storage time of the cavity is then

$$\tau_s = \frac{\tau_t}{1 - |r_1 r_2|} \approx \frac{2L}{cT_1} \tag{B.4}$$

where $\tau_t = L/c$ is the one-way transit time in the cavity. The change in optical phase of the reflected field for a unit change in cavity length near resonance is

$$\frac{\Delta\varphi}{\Delta L} \cong \frac{-16\pi}{\lambda_o T_1 \left[1 - (\frac{A_1+A_2}{T_1})^2\right]} \approx \frac{-8\pi}{\lambda_o} \frac{\tau_s}{\tau_t}. \tag{B.5}$$

The amplitude of the net reflected field at cavity resonance is

$$\frac{E_r}{E_0} = 1 - \frac{2(A_1 + A_2)}{T_1} \tag{B.6}$$

when the mirror optical losses are much smaller than the input mirror transmission.

2. The Gravitational Wave Transfer Function of the Interferometric Detector.

This section outlines the response of an interferometric gravitational wave detector ("interferometer") that uses Fabry-Perot cavities as the optical storage elements. We compute the responses to a sinusoidal wave incident from an arbitrary direction. The end result is the "transfer function" of the interferometer, defined as the complex ratio of the optical phase shift at the output (the antisymmetric port) of the interferometer at the gravitational wave frequency, f, to an excitation by a gravitational wave with amplitude h at frequency f.

In our calculation the interferometer masses are idealized as free (a good idealization above the resonant frequencies of the mass suspensions). The masses then travel along geodesics of the spacetime, which are distorted by the gravitational wave. We perform the calculation in "transverse traceless (TT) coordinates" [B–2]. In these coordinates the masses are forever at rest (x,y,z are constant on their geodesic world lines), and their coordinate separations are forever constant. However, the gravitational wave perturbs the metric of spacetime, thereby altering the masses' physical separations.

One interferometer mass is located at the origin and the other two are situated a distance L on the the x and y axes. The metric tensor is

$$g_{ij} = \eta_{ij} + h_{ij}(t, \vec{r}) \tag{B.7}$$

where η_{ij} is the flat spacetime Minkowski metric and $h_{ij}(t, \vec{r})$ is the metric perturbation produced by the gravitational wave. In TT coordinates h_{ij} is purely spatial ($h_{tj} = 0$), and the components that are relevant to our calculation are [B–2]

$$h_{xx} = h\, G_{xx} e^{(i\vec{k}\cdot\vec{r} - i\omega t)}, \qquad h_{yy} = h\, G_{yy} e^{(i\vec{k}\cdot\vec{r} - i\omega t)} \tag{B.8}$$

where

$$\begin{aligned} G_{xx} &\equiv \cos\,2\,\Omega\,(\cos^2\phi - \,\sin^2\phi\,\cos^2\theta)\,-\,\sin\,2\,\Omega\,\sin 2\,\phi\,\cos\,\theta \\ G_{yy} &\equiv \cos\,2\,\Omega\,(\sin^2\phi - \,\cos^2\phi\,\cos^2\theta)\,+\,\sin\,2\,\Omega\,\sin 2\,\phi\,\cos\,\theta. \end{aligned} \tag{B.9}$$

Here h is the gravitational wave strain in the plane perpendicular to the propagation direction and $\vec{k}$ is the wave vector,

$$\vec{k} \;=\; \frac{\omega}{c}\;(\;\sin\theta\,\sin\phi\vec{x}\;-\;\sin\theta\,\cos\phi\vec{y}\;+\;\cos\theta\vec{z}\;). \tag{B.10}$$

The polarization of the wave is specified by the angle Ω. We can think of $\Omega = 0$ as being the + polarization state and $\Omega = \pi/4$ as being the $\times$ state.

Now consider a photon traveling between the central mass and the mass located at $x \;=\; L$. The equation $ds^2 = g_{ij}dx^i dx^j = 0$, which expresses the fact that the photon travels at the speed of light, takes the following form, accurate to first order in the wave amplitude h:

$$c\frac{dt}{dx} \;=\; \pm(1 + \tfrac{1}{2}h_{xx}). \tag{B.11}$$

By integrating this equation along the photon's world line as it travels from the central mass at time t_0 to the end mass and back, we obtain for the time t of its return to the central mass

$$t \;=\; t_0 + 2\tau_t + \frac{\tau_t h G_{xx}}{2} H(\omega, k_x) e^{-i\omega(t_0+\tau_t)}. \tag{B.12}$$

Here $\tau_t = L/c$,

$$H(\omega, k_x) \;=\; \mathrm{sinc}\tfrac{1}{2}(k_x L - \omega\tau_t)e^{\frac{i}{2}(k_x L+\omega\tau_t)} \;+\; \mathrm{sinc}\tfrac{1}{2}(k_x L + \omega\tau_t)e^{\frac{i}{2}(k_x L-\omega\tau_t)}, \tag{B.13}$$

and $\mathrm{sinc}\; z \;=\; \mathrm{sin}z/z$.

A similar calculation is carried out for the light leaving the central mass at time t_0 that travels back and forth along the y direction. The difference in transit time for the two paths is given by

$$\Delta t \;=\; \frac{h\tau_t}{2}\big[G_{xx}H(\omega, k_x) \;-\; G_{yy}H(\omega, k_y)\big]e^{-i\omega(t_0+\tau_t)}. \tag{B.14}$$

Because the gravitational wave has $h_{tt} = 0$ and the central mass remains always at rest in the coordinate system, this Δt is equal to the proper time difference as measured by a physical clock riding on the central mass. The optical phase shift at the antisymmetric port of the interferometer due to to this time difference is

$$\Delta\phi^{(1)} \;=\; \omega\Delta t \;=\; \frac{2\pi c\Delta t}{\lambda} \tag{B.15}$$

where λ is the optical wavelength.

For the Fabry-Perot cavity the procedure is applied iteratively to the terms that transit the cavity multiple times. When the cavity is on resonance the unperturbed phase shift for each transit is a multiple of 2π. The perturbed phase shifts are small enough so that $e^{i\Delta\phi^{(1)}}$ is well approximated by $1 + i\Delta\phi^{(1)}$ and can be summed over the infinite series of transits.

After some algebraic manipulation, the transfer function of the recombined Fabry-Perot interferometer is found to be given by

$$\begin{aligned}\frac{\phi(f)}{h(f)} =& \frac{4\pi c\tau_t^2}{\lambda\tau_s}\left[G_{xx}H(\omega,k_x) - G_{yy}H(\omega,k_y)\right] \\ &\times\left(\frac{e^{i\omega\tau_t}}{1-2(1-\tau_t/\tau_s)e^{i\omega\tau_t}\cos(\omega\tau_t)+(1-\tau_t/\tau_s)^2e^{i2\omega\tau_t}}\right)\end{aligned} \tag{B.16}$$

The transfer function simplifies at low gravitational wave frequencies, $f < 1/4\pi\tau_t$, and for optimal source direction ($\theta = \phi = 0$) and polarization ($\Omega = 0$). For this case it is

$$\frac{\phi}{h}(f) \approx \left(\frac{8\pi c\tau_s}{\lambda}\right)\frac{1}{\left(1+(2\omega\tau_s)^2\right)^{1/2}}. \tag{B.17}$$

At other angles of incidence the angular dependence of the interferometer is primarily determined by $G_{xx} - G_{yy}$.

Figure B–2 shows the amplitude response of an interferometric gravitational wave detector as a function of the propagation direction of the wave relative to the plane of the detector. The response has been averaged over the wave polarization angle (Ω).

3. Basic Optical Concepts and RF Phase Modulation.

In this section a rudimentary description of the basic optical concepts of an interferometer, such as that shown in Section III, Figure III–1, is given. The analysis makes many simplifying assumptions, the most important being that only a single mode and polarization of the light are considered. The Fabry-Perot cavities are assumed to be close enough to resonance that their phase response can be linearized, and the RF modulation has small enough amplitude that it too can be linearized.

The analysis is intended to show the steps involved in the propagation of the optical wave field from the beam splitter, through the RF phase modulators, reflection from the Fabry-Perot cavities, to recombination at the second encounter with the beam splitter, and finally to the photodiode at the antisymmetric port of the interferometer, which monitors the output signal of the system.

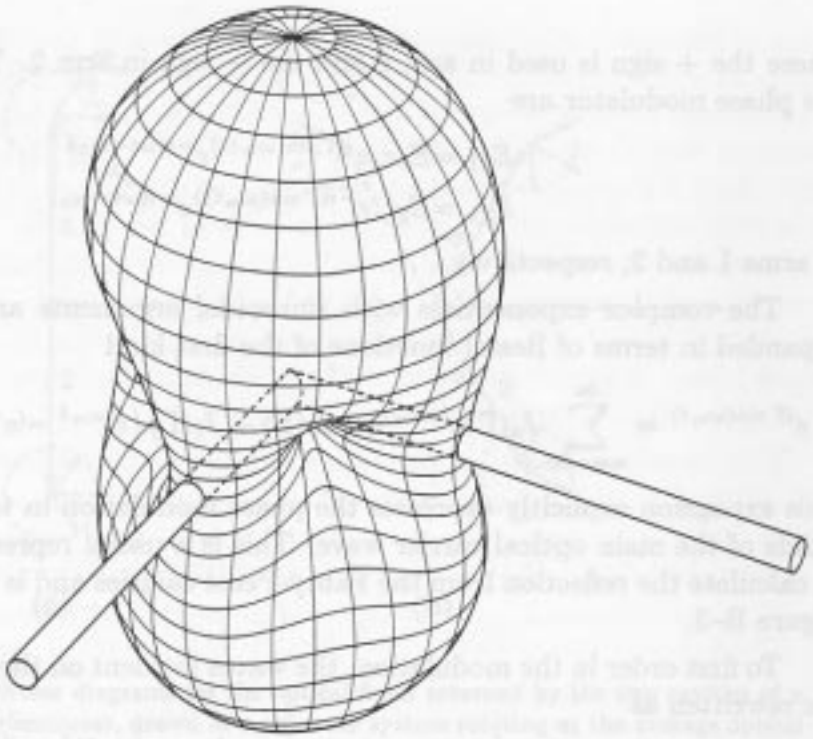

Figure B–2 The angular response pattern of an interferometer with orthogonal arms to unpolarized gravitational radiation. The tubes penetrating the response pattern surface represent the interferometer arms.

The time dependence of the input light at the beam splitter is given by

$$E = E_0 e^{-i\omega t}. \tag{B.18}$$

The two waves leaving the beam splitter are

$$\begin{aligned} E_{10} &= r_s E \quad \text{the wave launched into arm 1,} \\ E_{20} &= t_s E \quad \text{the wave launched into arm 2,} \end{aligned} \tag{B.19}$$

where t_s and r_s are the transmission and reflection coefficients of the beam splitter. The two waves next pass through optical phase modulators which are crystals with the property that their optical index of refraction is linearly proportional to an applied modulating field (Pockels effect). The modulating field is chosen to be at a radio frequency (RF), ω_m, sufficiently high that the laser amplitude noise and the noise in the photodetection circuitry at this frequency are close to fundamental limits. The phase modulation adds a time dependent phase to the optical beams given by

$$\phi(t) = \pm\Gamma\sin(\omega_m t), \tag{B.20}$$

where the + sign is used in arm 1 and the − sign in arm 2. The wave fields after the phase modulator are

$$\begin{aligned} E_{11} =& E_0 r_s e^{i(\Gamma \sin(\omega_m t))} e^{-i(\omega t - \delta_{11})} \\ E_{21} =& E_0 t_s e^{-i(\Gamma \sin(\omega_m t))} e^{-i(\omega t - \delta_{21})} \end{aligned} \tag{B.21}$$

in arms 1 and 2, respectively.

The complex exponentials with sinusoidal arguments are most conveniently expanded in terms of Bessel functions of the first kind

$$e^{i\Gamma \sin(\omega_m t)} = \sum_{n=-\infty}^{\infty} J_n(\Gamma) e^{in\omega_m t} \approx J_0(\Gamma) + J_1(\Gamma)\left(e^{i\omega_m t} - e^{-i\omega_m t}\right) + \cdots \tag{B.22}$$

This expansion explicitly expresses the phase modulation in terms of a set of sidebands of the main optical carrier wave. This is a useful representation with which to calculate the reflection from the Fabry-Perot cavities and is shown graphically in Figure B–3.

To first order in the modulation, the waves incident on the Fabry-Perot cavities are rewritten as

$$\begin{aligned} E_{12} =& E_0 r_s \left[J_0(\Gamma) + J_1(\Gamma)\left(e^{i\omega_m t} - e^{-i\omega_m t}\right)\right] e^{-i(\omega t - \delta_{12})} \\ E_{22} =& E_0 t_s \left[J_0(\Gamma) - J_1(\Gamma)\left(e^{i\omega_m t} - e^{-i\omega_m t}\right)\right] e^{-i(\omega t - \delta_{22})}, \end{aligned} \tag{B.23}$$

in arms 1 and 2, respectively.

The reflection coefficients of the cavities given by Equation B.3 are rewritten in terms of an amplitude and phase

$$r_j = A_j(\omega_j, \omega_l) e^{i\phi_j(\omega_j, \omega_l)} \tag{B.24}$$

The index j takes on the value 1 or 2 indicating the cavity, ω_j is the resonance frequency of the cavity and ω_l is the frequency of the light. The gravitational wave affects the phases ϕ_j.

The waves after reflection from the cavities become

$$\begin{aligned} E_{13} =& E_0 r_s \Big[J_0(\Gamma) A_1(\omega_1, \omega) e^{i\phi_1(\omega_1, \omega)} + J_1(\Gamma) \\ & \times \left(A_1(\omega_1, \omega + \omega_m) e^{i\phi_1(\omega_1, \omega+\omega_m)} e^{i(\omega_m t + \delta_{1+})} \right. \\ & \left. - A_1(\omega_1, \omega - \omega_m) e^{i\phi_1(\omega_1, \omega-\omega_m)} e^{-i(\omega_m t - \delta_{1-})} \right) \Big] e^{-i(\omega t - \delta_{13})} \end{aligned} \tag{B.25}$$

in arm 1 and

$$\begin{aligned} E_{23} =& E_0 t_s \Big[J_0(\Gamma) A_2(\omega_2, \omega) e^{i\phi_2(\omega_2, \omega)} - J_1(\Gamma) \\ & \times \left(A_1(\omega_2, \omega + \omega_m) e^{i\phi_2(\omega_2, \omega+\omega_m)} e^{i(\omega_m t + \delta_{2+})} \right. \\ & \left. - A_2(\omega_2, \omega - \omega_m) e^{i\phi_2(\omega_2, \omega-\omega_m)} e^{-i(\omega_m t - \delta_{2-})} \right) \Big] e^{-i(\omega t - \delta_{23})} \end{aligned} \tag{B.26}$$

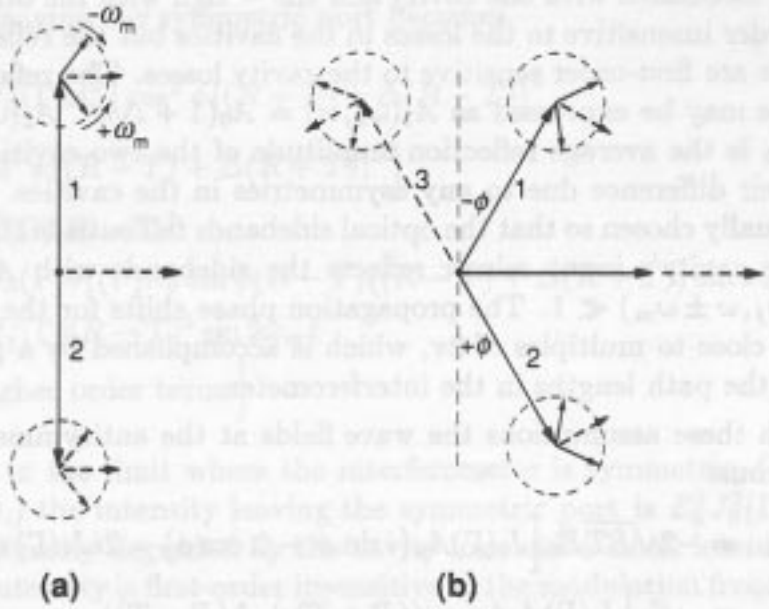

Figure B–3 Phasor diagrams for the optical fields returned by the two cavities of a Fabry–Perot interferometer, drawn in a reference system rotating at the average optical frequency, ω. The labels 1, 2, and 3 each denote a field complex composed of a stationary component (the long vectors), corresponding to a main optical field, and components rotating at $\pm\omega_m$ (the short vectors), which correspond to phase modulation sidebands. In (a) the field at the antisymmetric port is shown when cavities 1 and 2 are on resonance. The resultant field (sum of 1 and 2) is a small oscillating field due to the modulation (the dashed line). The intensity in this case has a small average value and a component at $2\omega_m$ but no component at ω_m. In (b), the interaction with a gravitational wave, produces opposing phase shifts in the two arms of the interferometer, each with magnitude ϕ. The resultant of the fields 1 and 2 is the total field at the antisymmetric output, which has both an average value (the solid line) and an oscillating component (the dashed line). The intensity now includes a term proportional to ϕ at ω_m. An additional set of vectors, labelled 3, depicts the field from arm 2 that appears at the symmetric port. The resultant of 1 and 3 is the total field at the symmetric port. When $\phi \approx 0$, the resultant field is approximately equal to the input field without modulation. This is the field that gets recycled.

in arm 2. Here δ_{1+}, δ_{1-} (or δ_{2+}, δ_{2-}) are small phase shifts that depend on the sum and difference modulation frequencies, respectively, for cavity 1 (or cavity 2).

After reflection from the cavities the waves are recombined at the beam splitter. The wave leaving the antisymmetric port of the splitter, given by $E_{\rm anti} = t_s E_{13} - r_s E_{23}$ is detected on the output photodetector. The wave leaving the symmetric port of the splitter, given by $E_{\rm sym} = r_s E_{13} + t_s E_{23}$ returns to the recycling mirror or laser depending on the interferometer configuration.

When the Fabry-Perot cavities are operated close to resonance, $\omega \approx \omega_j$, the reflected wave at the main optical carrier of frequency ω suffers a phase shift of $\pi \pm \phi$ (refer to Figure B–1). Here ϕ is the phase shift due to the gravitational wave; the

+ sign is associated with one cavity and the − sign with the other. The phase shift is first order insensitive to the losses in the cavities but the reflection amplitudes at resonance are first order sensitive to the cavity losses. The reflection amplitudes at resonance may be expressed as $A_1(\omega_1,\omega) = A_0(1+\Delta), \quad A_2(\omega_2,\omega) = A_0(1-\Delta)$, where A_0 is the average reflection amplitude of the two cavities at resonance and 2Δ is their difference due to any asymmetries in the cavities. The RF frequency, ω_m, is usually chosen so that the optical sidebands fall outside the cavity resonances. Then the cavity's input mirror reflects the sidebands with $A_j(\omega_j,\omega\pm\omega_m)\approx 1$ and $\phi_j(\omega_j,\omega\pm\omega_m) \ll 1$. The propagation phase shifts for the sidebands, $\delta_{k\pm}$,are assumed close to multiples of 2π, which is accomplished by a proper choice of ω_m knowing the path lengths in the interferometer.

With these assumptions the wave fields at the antisymmetric and symmetric ports become

$$\begin{aligned} E_{\rm anti} &= -2\sqrt{RT}E_0\Big[J_0(\Gamma)A_0\big(i\sin\phi+\Delta\cos\phi\big) - 2iJ_1(\Gamma)\sin\omega_m t\Big] \\ E_{\rm sym} &= -E_0\Big[J_0(\Gamma)A_0\big(\cos\phi((R+T)+\Delta(R-T)) \\ &\qquad + i\sin\phi((R-T)+\Delta(R+T))\big) \\ &\qquad - 2iJ_1(\Gamma)(R-T)\sin\omega_m t\Big] \end{aligned} \tag{B.27}$$

where $R = r_s^2$ and $T = t_s^2$ are the intensity reflection and transmission of the beam splitter. These fields are shown in Figure B–3. Terms that oscillate at the modulation frequency are shown with dashed lines.

The intensity is proportional to the envelope of the field given by $I = |E|^2$. The intensity at the output photodetector (antisymmetric port) becomes

$$\begin{aligned} I_{\rm anti}(t) =& 4RTE_0^2\big[J_0^2(\Gamma)A_0^2(\sin^2\phi+\Delta^2\cos^2\phi) + 2J_1^2(\Gamma) \\ &+ \text{higher order time independent terms}\big] \\ &- 4RTE_0^2\big[4J_0(\Gamma)J_1(\Gamma)A_0\sin\phi\sin\omega_m t - 2J_1^2(\Gamma)\cos 2\omega_m t \\ &+ \text{higher order time dependent terms.}\big] \end{aligned} \tag{B.28}$$

The interferometer output signal is the term associated with $\sin\omega_m t$, which after synchronous demodulation and for $\phi < 1$ is linearly proportional to ϕ, the gravitational wave induced phase shift. The time independent terms make up the background light on the photodetector. They are important in estimating the interferometer's photon shot noise limit. In a completely balanced interferometer with perfect contrast, $\Delta = 0$, the average background intensity becomes $2RTE_0^2(1-J_0(2\Gamma))$ when $\phi = 0$. The small average intensity remaining in the dark fringe is then entirely due to the modulation: for $\Gamma \ll 1$, it is[1] $2RTE_0^2\Gamma^2$.

[1] For small values of Γ the first two Bessel functions of the first kind are $J_0(\Gamma)\approx 1-\Gamma^2/4$ and $J_1(\Gamma)\approx\Gamma/2$.

The intensity leaving the symmetric port becomes

$$\begin{aligned} I_{\rm sym} =& E_0^2\Big[J_0^2(\Gamma)A_0^2\Big(\cos^2\phi\big((R+T)+\Delta(R-T)\big)^2 \\ &+\sin^2\phi\big((R-T)+\Delta(R+T)\big)^2\Big) \\ &+J_1^2(\Gamma)(R-T)^2 \\ &-4J_0(\Gamma)J_1(\Gamma)A_0\sin\phi(R-T)\big((R-T)+\Delta(R+T)\big)\sin\omega_m t \\ &-2J_1^2(\Gamma)(R-T)^2\sin 2\omega_m t \\ &+\text{higher order terms}\Big] \end{aligned} \tag{B.29}$$

To first order in Γ in the limit where the interferometer is symmetric, ($R = T = 0.5$, $\Delta = 0$, $\phi = 0$,) the intensity leaving the symmetric port is $E_0^2 J_0^2(\Gamma)A_0^2$ This is just the input intensity degraded by the cavity loss and a small loss due to the modulation. This intensity is first-order insensitive to the modulation frequency and the gravitational wave induced phase shift ϕ. Figure B–3 shows this geometrically.

4. The Physical Basis of Some of the Noise Terms.

In this section we discuss the photon shot noise, the effect of laser frequency noise, the fluctuations in the forward scattering of the residual gas, the thermal noise, and the optical radiation pressure fluctuations that enforce the standard quantum limit. Seismic noise is discussed separately in Appendix D.

a. Photon shot noise. Photon shot noise, which can be thought of as due to the counting statistics of the photons, dominates the estimated noise budget at high frequencies. The uncertainty in the optical phase and the uncertainty in the number of photons in a specific state of the radiation field are related by the electromagnetic uncertainty relation $\Delta\phi\Delta n > 1$. In the coherent state of single-mode laser light, the photons have a Poisson distribution: $\Delta n = \sqrt{< n >}$ The amplitude spectral density of the photon "current" at frequency f is given by

$$\frac{dn}{dt}(f) = \left(2\left\langle\frac{\delta n}{\delta t}\right\rangle\right)^{1/2} \tag{B.30}$$

The resultant phase fluctuations, expressed as an optical phase amplitude density at the antisymmetric output of the interferometer, is given by

$$\tilde{\phi}_n(f) = \left(\frac{2{\rm h}c}{\lambda\eta\epsilon P(1-L_{opt})G_R}\right) \tag{B.31}$$

Here η=detector quantum efficiency, ϵ=optical efficiency of the entire optical train, P=laser optical power, $L_{\rm opt}$=total optical loss $\geq 4Ac\tau_s/L$, A=average loss per

mirror, G_R=broadband recycling power gain $\leq 1/L_{\rm opt}$ ($G_R = 1$ for no recycling), λ=optical wavelength, h=Planck's constant.

The interferometer's shot noise limited sensitivity expressed as an equivalent gravitational wave strain amplitude, is given from Equations B.17 and B.31 by

$$\tilde{h}(f) = \tilde{\phi}_n(f)\left[\frac{\phi}{h}(f)\right]^{-1} \tag{B.32}$$

For a Fabry-Perot interferometer without recycling this becomes

$$\tilde{h}(f) = f_0\left(\frac{\mathrm{h}\lambda}{\eta\epsilon P(1-L_{\rm opt})c}\right)^{1/2}\left[1+(f/f_0)^2\right]^{1/2} . \tag{B.33}$$

where $f_0 = 1/4\pi\tau_s$, and τ_s is the energy light storage time for each arm's cavity. This result includes a factor of 2 for recovery of the phase information from the RF modulation techniques used in a practical interferometer. The shot noise contribution becomes independent of the storage time at gravitational wave frequencies greater than f_0, so there is no penalty in using large storage times.

For broadband recycling, under the optimum assumption that all the optical loss in the system is due to the loss in the cavity mirrors, the shot noise limit is

$$\tilde{h}(f) = f_0^{1/2}\left(\frac{cA}{\pi L}\right)^{1/2}\left(\frac{\mathrm{h}\lambda}{\eta\epsilon P(1-L_{\rm opt})c}\right)^{1/2}\left[1+(f/f_0)^2\right]^{1/2} . \tag{B.34}$$

In a broadband recycled system the sensitivity is optimized at a frequency f by choosing the storage time so that $\tau_s = 1/4\pi f$, i.e. so that $f = f_0$.

b. Frequency fluctuations of the laser. Fluctuations in the frequency of the laser can contribute to the interferometer's phase noise in two ways: (i) Frequency fluctuations can couple to a difference in the storage times of the two Fabry-Perot cavities to produce a gravitational strain noise $\tilde{h}(f) = 2\tilde{\nu}(f)\Delta\tau/\nu\tau$, where $\tilde{\nu}(f)$ = amplitude spectrum of frequency fluctuations, ν = laser frequency, $\Delta\tau/\tau$ = fractional storage time unbalance of the two cavities. This noise can be reduced by electronically differencing the cavity locking signals and the antisymmetric output, since frequency noise is common to them. (ii) Frequency noise can introduce relative phase fluctuations between the main beam in a cavity and scattered-light beams, thereby enhancing scatter-light noise. Methods for controlling this are discussed in Appendix F.

c. Noise from the residual gas. The residual gas can produce mechanical noise in the interferometer by damping the suspensions (see below) and by producing acoustic coupling to the outside world. This mechanical noise will be reduced to a negligible level in the LIGO by operating at pressures less than 10^{-6} torr. More serious are fluctuations in forward scattering of light by residual gas in the beam

tubes. The gravitational wave noise due to fluctuations in scattering is calculated by determining the overlap of the forward scattered fields of each molecule in the beam with the main field mode at the photodetector. The scattered field of the individual molecules appears as pulses with different amplitudes and pulse lengths depending on the molecule's position and velocity transverse to the main beam axis. The power spectrum of these pulses, when averaged over all the molecules residing in the beam with a Maxwell distribution of molecular speeds, gives a gravitational-phase noise of

$$\tilde{h}_{\rm total}(f) = \frac{2^{5/2}\pi^{5/4}\alpha(\omega_{opt})\rho_{\#}^{1/2}}{b^{1/2}v_0^{1/2}\lambda^{1/4}L^{3/4}} \quad e^{-\sqrt{2\pi}\, f(\lambda L)^{1/2}/v_o}. \qquad \text{(B.35)}$$

This expression assumes that the optical beam radius is the minimum allowed by the length L of an interferometer arm. In this expression α is the polarizability of the residual gas molecule at the optical frequency ω_{opt}, $\rho_{\#}$ is the average number of molecules per unit volume, v_0 is the average thermal velocity of the molecule, λ is the wavelength of the light and b is the number of light beams (for a Fabry-Perot interferometer, $b = 1$). Figure B–4 shows the numerical results for various gas species.

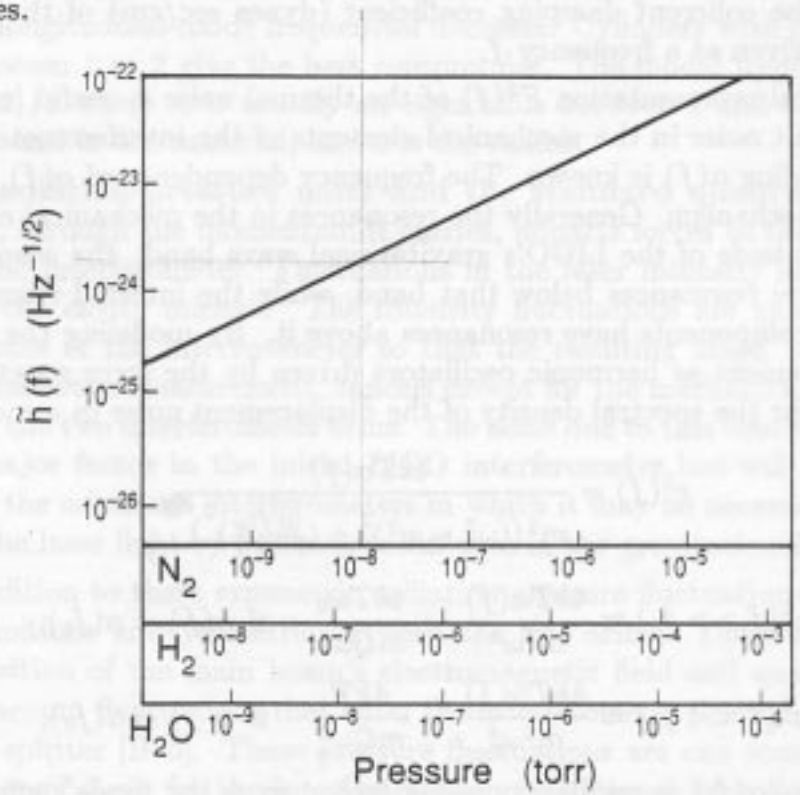

Figure B–4 Noise due to statistical fluctuations in the index of refraction of the residual gas in the LIGO beam tubes, expressed as an equivalent gravitational-wave strain amplitude spectral density $\tilde{h}(f)$. This noise is nearly independent of frequency over the LIGO's frequency band. The contribution to $\tilde{h}(f)$ is plotted as a function of partial pressure for various gas species.

d. Thermal noise. The fluctuation-dissipation theorem of statistical mechanics [B–3] asserts that the damping mechanism in a physical system produces thermally driven random fluctuations in the system's modes of motion. The theorem is easy to understand in the case of the damping of a mechanical system by residual gas. The damping mechanism is the coherent transfer of momentum from the moving object to the residual gas particles (Doppler friction), while the fluctuations are imparted to the object by the random impacts of the residual gas particles, which are thermalized at temperature T.

The residual gas in the LIGO is specified to be low enough so that it does not contribute to the dissipation of the LIGO's mechanical elements (mirrors, masses, beam splitters, ...). The principle sources of thermal noise are expected to be dissipation in the flexure of the suspension support elements and the internal dissipation of the normal modes of the cavity mirrors.

Thermal noise in a mechanical system can be expressed as

$$F^2(f) = 4kT\alpha(f) \qquad \text{dynes}^2/\text{Hz}. \tag{B.36}$$

Here $\alpha(f)$ is the coherent damping coefficient (dynes sec/cm) of the mechanical system when driven at a frequency f.

The spectral representation $F^2(f)$ of the thermal noise is useful in estimating the displacement noise in the mechanical elements of the interferometer at all frequencies, providing $\alpha(f)$ is known. The frequency dependence of $\alpha(f)$ depends on the damping mechanism. Generally the resonances in the mechanical elements are chosen to be outside of the LIGO's gravitational wave band: the suspensions are designed to have resonances below that band, while the internal resonant modes of the optical components have resonances above it. By modeling the mechanical modes of an element as harmonic oscillators driven by the force spectral density, one computes for the spectral density of the displacement noise in a mode

$$x^2(f) = \frac{4kT\alpha(f)}{m^2\left((\omega_0^2 - \omega^2)^2 + \left(\frac{\alpha(f)\omega}{m}\right)^2\right)^2}, \tag{B.37}$$

$$x^2(f >> f_0) \approx \frac{4kT\alpha(f)}{m^2\omega^4} \rightarrow \frac{4kT\omega_0}{mQ\omega^4} \quad \text{if } \alpha(f) = \alpha(f_0), \tag{B.38}$$

$$x^2(f << f_0) \approx \frac{4kT\alpha(f)}{m^2\omega_0^4} \rightarrow \frac{4kT}{mQ\omega^3} \quad \text{if } \alpha(f) = \alpha(f_0), \tag{B.39}$$

where $Q = m\omega_0/\alpha(f_0)$ = oscillator quality factor, m = the mode's effective mass, $\omega_0 = 2\pi f_0$ = the mode's resonance frequency.

In estimating the equivalent gravitational strain noise due to the thermal noise from several elements, assumed uncorrelated, the noise power is summed

$$h^2(f) = \frac{\sum_{n=1}^{m} x^2(f)}{L^2} \tag{B.40}$$

Several subtleties arise in estimating the thermal noise: (i) As indicated, the damping can be frequency dependent so that a simple measurement of the Q of an oscillator is not sufficient to predict the thermal noise off resonance. (ii) In an oscillator under the influence of several restoring mechanisms, such as in a pendulum where both gravity and the elasticity of the suspension fibers apply restoring forces, the Q of the entire mechanical system can be much larger than the intrinsic Q of the suspension fiber material. The Q of the pendulum is larger than the Q of the suspension material by the ratio of the energy stored in the gravitational field to that stored in the elastic deformation of the fiber. (iii) Estimates of the equivalent gravitational wave strain due to thermal excitation of the normal modes of the test masses and mirrors depend on the overlap integral of the optical mode shape with the mechanical mode of the mass. The test masses and mirrors in the gravitational wave interferometer will usually be cylinders. The modal frequencies and shapes for cylinders with radii comparable to their height have been studied extensively [B–4]. The most perturbative modes are those that cause a net phase shift over a large part of the optical wavefront and are at the lowest frequencies. The lower order flexural modes tend to increase in frequency with cylinder height, while the longitudinal mode frequencies decrease. Cylinders with ratio of height to radius between 1 to 2 give the best compromise. The modal frequencies are given by $f = \Lambda v_s/a$ where Λ is usually an eigenvalue between 1 and 5, v_s is the shear speed of sound in the material, and a is the radius.

e. Radiation pressure noise and the standard quantum limit. The laser light, through the momentum it carries, imparts forces to the optical components of the interferometer. Fluctuations in the laser intensity introduce random forces on the cavity mirrors. The intensity fluctuations are symmetric between the two arms of the interferometer so that the resulting noise, which affects the gravitational wave measurement, cancels except for the mechanical and optical unbalance of the two interferometer arms. The noise due to this source is not expected to be a major factor in the initial LIGO interferometer but will have to be considered in the advanced interferometers in which it may be necessary to amplitude stabilize the laser light by feedback techniques in the gravitational wave band.

In addition to these symmetric radiation pressure fluctuations, there are pressure fluctuations antisymmetric between the two arms. These are produced by a superposition of the main beam's electromagnetic field and quantum electrodynamical vacuum fluctuations that enter the interferometer through the dark side of the beam splitter [B–5]. These pressure fluctuations are one source of the "standard quantum" limit for the interferometric gravitational detector and are a macroscopic example of the "Heisenberg microscope." Because the fluctuating radiation pressure is proportional to the correlated product of the vacuum field and the laser field, it varies as the square root of the laser power and fluctuates on time scales of the cavity storage time, a characteristic time for the vacuum electric fluctuations to change phase by π relative to the laser field.

Following this model, the rms fluctuating differential force on the pair of mirrors in one cavity is

$$\Delta F = \sqrt{< N >}\left[\frac{\mathrm{h}\nu}{L}\right] \tag{B.41}$$

where $< N >$ is the average number of quanta stored in the cavity mode and L is the cavity length. The spectral density of the fluctuating force is determined from

$$(\Delta F)^2 = \int_0^{1/2\tau} F^2(f) df,$$

where

$$F^2(f) = 2\tau(\Delta F)^2 = 2\tau < N > \left(\frac{\mathrm{h}\nu}{L}\right)^2,$$

$$\tau \approx \frac{2L}{cT},$$

$$F^2(f) = \frac{4 < N > (\mathrm{h}\nu)^2}{cTL}, \tag{B.42}$$

and we assume negligible losses in the cavity's central mirror, $A \ll T$. Assuming that the mirror masses, m, can be considered free, the force produces a differential motion $x(f) \approx F(f)/m\omega^2$. The average number of quanta in the mode and the laser power are related by

$$< N >= \frac{2LP_{\mathrm{in}}}{cT\mathrm{h}\nu}, \tag{B.43}$$

$$P_{\mathrm{in}} = \frac{\epsilon_{\mathrm{opt}} P_{\mathrm{laser}}}{2}, \tag{B.44}$$

where it is assumed that the beam splitter divides the input power evenly between the two cavities. Finally, the equivalent gravitational strain noise induced in both cavities is

$$\begin{aligned} \tilde{h}(f)_{\mathrm{pressure}} &= \frac{\sqrt{2}x(f)}{L} \\ &= \frac{4(\epsilon_{\mathrm{opt}} P_{\mathrm{laser}} \mathrm{h}\nu)^{1/2}}{cTLm\omega^2} \end{aligned} \tag{B.45}$$

The sensing noise (shot noise) in the detection of the interferometer fringe at low frequencies is

$$\tilde{h}(f)_{\mathrm{sense}} = \frac{T}{8\pi L}\left(\frac{\mathrm{h}\lambda c}{\eta\epsilon_{\mathrm{opt}} P_{\mathrm{laser}}}\right)^{1/2}. \tag{B.46}$$

The total noise of the interferometer if only due to optical field fluctuations is the incoherent sum

$$h^2(f) = h^2_{\mathrm{pressure}}(f) + h^2_{\mathrm{sense}}(f). \tag{B.47}$$

Since the radiation pressure noise power varies directly as the laser power, while the sensing noise varies inversely as the laser power, there is a minimum in the total noise at a specific, optimum laser power given by

$$P_{\rm opt} = \frac{T^2 \lambda m c \omega^2}{32\pi\epsilon_{\rm opt}\eta^{1/2}} = \frac{L^2 \lambda m \omega^4}{2\pi\epsilon_{\rm opt} c \eta^{1/2}}. \tag{B.48}$$

The term on the right reexpresses the optimum input power in terms of the optimum cavity input mirror transmission for a gravitational wave frequency at $\omega = 2\pi f$. This is given by $T_{\rm opt} = 4L\omega/c$. One contribution to the standard quantum limit for an interferometric detector at a gravitational wave frequency f is the net pressure and sensing noise at the optimized power with photodetector efficiency $\eta = 1$. The quantum limit is actually $\sqrt{2}$ larger than that net noise, because of a contribution from the uncertainty principle associated with the center-of-mass motion of the mirrors [B–5]:

$$\tilde{h}(f)_{\rm QL} = \sqrt{4/\pi}\left(\frac{\rm h}{m}\right)^{1/2} \frac{1}{2\pi f L} \tag{B.49}$$

This noise is shown in Section V, Figure V–3 for the initial LIGO interferometer and Figure V–4 for an advanced detector. The quantum noise is not a factor in the initial interferometers but it does set a fundamental limit to the technique and is one of the reasons along with all other sources of random forces that argues for a large arm length L.

There are methods, in principle, for circumventing the standard quantum limit in interferometers but it is not at all clear whether these methods can be realized in practice.

References

[B–1] See, e.g., J.-Y. Vinet, B. Meers, C. N. Man, and A. Brillet, *Physical Review D* **38**, 433 (1988), and references cited therein.

[B–2] See, e.g., L. D. Landau and E. M. Lifschitz, *The Classical Theory of Fields* (Pergamon Press, Oxford, 1962); or C. W. Misner, K. S. Thorne, and J. A. Wheeler, *Gravitation* (W.H. Freeman, San Francisco, 1973).

[B–3] F. Reif, *Fundamentals of Statistical and Thermal Physics* (McGraw-Hill, New York, 1965).

[B–4] J. Hutchinson, *Journal of Applied Mechanics* **47**, 901, (1980); G. McMahon, *Journal of the Acoustical Society of America* **36**, 85, (1964).

[B–5] C. M. Caves, *Physical Review D,* **23**, 1693 (1981).

appb1119ef.tex